Revision_1

Order of $^{[6]}Ti^{4+}$ in a Ti-rich calcium amphibole from Kaersut, Greenland: a combined X-ray and neutron diffraction study

G. Diego Gatta, Garry J. McIntyre, Roberta Oberti and Frank C. Hawthorne

Running title: Order of $^{[6]}Ti^{4+}$ in Ti-rich calcium amphibole

Corresponding author: G. Diego GATTA
Dipartimento di Scienze della Terra, Università degli Studi di Milano
Via Botticelli 23, I-20133 Milano, Italy
Tel. +39 02 503 15607, Fax +39 02 503 15597, E-Mail: diego.gatta@unimi.it

Manuscript submitted to Physics and Chemistry of Minerals

Order of $^{[6]}Ti^{4+}$ in a Ti-rich calcium amphibole from Kaersut, Greenland: a combined X-ray and neutron diffraction study

G. Diego Gatta[1], Garry J. McIntyre[2], Roberta Oberti[3], Frank C. Hawthorne[4]

[1]Dipartimento di Scienze della Terra, Università degli Studi di Milano,
Via Botticelli 23, I-20133 Milano, Italy
[2]Australian Nuclear Science and Technology Organisation, New Illawarra Road,
Lucas Heights NSW 2234, Australia
[3]CNR-Istituto di Geoscienze e Georisorse, Via Ferrata 1, I-27100 Pavia
[4]Department of Geological Sciences, University of Manitoba, Winnipeg, Canada R3T 2N2

Abstract

In order to characterize the role of Ti in the crystal structure of calcium amphiboles with high or even dominant oxo-component, the crystal structure of a Ti-rich calcium amphibole from a gabbro at Kaersut, Greenland, has been refined with single-crystal Mo*K*α X-ray intensity data to an $R_1(F)$ index of ~ 0.025, and with single-crystal Laue neutron intensity data to an $R_1(F)$ index of ~ 0.053. The crystal used for X-ray structure refinement was characterized by electron- and ion-microprobe analysis. The site populations of the C-group cations Mg, Fe and Ti were calculated from the refined site-scattering values for the *M*(1), *M*(2) and *M*(3) sites derived by both X-ray and neutron diffraction. Ti is distributed among all the three 6-fold coordinated *M* sites, with a strong preference for the *M*(1) and *M*(3) sites, where its main role is maintaining electroneutrality at the deprotonated O(3) site. The pattern of distortion of the *M*(1), *M*(2) and *M*(3) octahedra differs from that in F-free deprotonated or partly deprotonated amphiboles, where Ti^{4+} does not occur at the *M*(3) site. The neutron structure refinement provides also a clear picture of the environment of the proton, anisotropic-displacement behaviour and potential hydrogen-bonding arrangements. A trifurcated hydrogen-bonding configuration has been identified, with two O(6) and one O(7) oxygen atoms as *acceptors* of weak hydrogen-bonds.

Keywords: Ti-rich amphibole, kaersutite, single-crystal X-ray diffraction, single-crystal Laue neutron diffraction, crystal chemistry.

Introduction

The amphiboles are probably the mineral supergroup with the highest chemical variability and the highest ability to crystallize under almost all the conditions relevant to petrogenesis. The general amphibole formula is written (Hawthorne and Oberti 2007) as

$$A_{0\text{-}1}\ B_2\ C_5\ T_8\ O_{22}\ W_2,$$

where: $A = Na^{+}, K^{+}, \square, Ca^{2+}, Li^{+}$;

$B = Na^{+}, Li^{+}, Ca^{2+}, Mn^{2+}, Fe^{2+}, Mg^{2+}$;

$C = Mg^{2+}, Fe^{2+}, Mn^{2+}, Al^{3+}, Fe^{3+}, Mn^{3+}, Ti^{4+}, Li^{+}$;

$T = Si^{4+}, Al^{3+}, Ti^{4+}$;

$W = (OH)^{-}, F^{-}, Cl^{-}, O^{2-}$.

With regard to the present work, C defines the cations occupying the octahedrally coordinated *M*(1), *M*(2) and *M*(3) sites and T defines the cations occupying the tetrahedrally coordinated *T*(1) and *T*(2) sites. The amphibole structure (with site nomenclature) is shown in Figure 1. Recent studies have shown that the oxo component, $^{W}O^{2-}$ or $^{O(3)}O^{2-}$ to identify the relvant site, is particularly important in affecting both the geometry and the crystal-chemical behaviour of the amphibole, to the extent that oxo-dominant compositions are now classified as a separate group by the current nomenclature scheme (Hawthorne et al. 2012).

The ability of the amphibole structure to incorporate cations in different coordinations and at different structural sites, particularly where related to coupled substitutions, makes this mineral supergroup the ideal case study to test crystal-chemical mechanisms controlling the incorporation of Ti^{4+} in silicates.

Previous work

Leake (1968) compiled a large number of amphibole analyses from the literature and classified them as to quality. Saxena and Ekström (1970) examined 639 analyses, all first-class and some second-class analyses as classified by Leake (1968), by principal component analysis. The strongest correlation between chemical variables in this dataset is between Ti^{4+} and $(OH)^{-}$. They proposed that Ti^{4+} enters calcium and sodium-calcium amphiboles *via* the substitution

$$Ti^{4+} + O^{2-} \rightarrow {}^{[6]}Al^{3+} + (OH)^{-} \qquad (1)$$

and found no correlation between the oxo component and the Fe^{3+} content of the amphibole.

Kitamura et al. (1975) and Pechar et al. (1989) showed by neutron diffraction that Ti is a C cation and is very strongly ordered at *M*(1) in two kaersutites. Oberti et al. (1992) showed by X-ray structure refinement that $^{[6]}Ti^{4+}$ is incorporated into the amphibole richterite structure *via* three distinct substitutions:

$$^{M(1)}Ti^{4+} + 2\ ^{O(3)}O^{2-} \rightarrow {}^{M(1)}Mg^{2+} + 2\ ^{O(3)}(OH)^{-} \quad (2)$$

$$^{M(2)}Ti^{4+} + 2\ ^{T(1)}Al^{3+} \rightarrow {}^{M(2)}(Mg,Fe)^{2+} + 2\ ^{T(1)}Si^{4+} \quad (3)$$

$$^{T(2)}Ti^{4+} \rightarrow {}^{T(2)}Si^{4+} \quad (4)$$

In richterites from lamproites, the partitioning between the C and T cation-groups depends on the pressure of crystallization (Konzett 1997; Konzett et al. 1997) and the F content of the amphibole (Della Ventura et al. 1991, 1993). In an examination of a series of synthetic Ti-rich Fe-free kaersutites by X-ray diffraction, Tiepolo et al. (1999) showed that $^{[6]}Ti$ is disordered over *M*(1), *M*(2) and *M*(3) with a strong preference for the *M*(1) site, and proposed two separate mechanisms for incorporation of ^{C}Ti into the amphibole structure: The first mechanism couples $^{[6]}Ti$ to the occurrence of O^{2-} at O(3) and leads to complete order of $^{[6]}Ti$ at *M*(1) (*i.e.*, substitution (2) above); the local association of $^{M(1)}Ti^{4+}$ with $2\ ^{O(3)}O^{2-}$ was confirmed spectroscopically by Della Ventura et al. (2007). The second substitution couples $^{[6]}Ti$ to the occurrence of Al at the *T* sites (*i.e.*, substitution (5) below):

$$^{M(2,3)}Ti^{4+} + 2\ ^{T(1,2)}Al^{3+} \rightarrow {}^{M(2,3)}Mg^{2+} + 2\ ^{T(1,2)}Si^{4+} \quad (5)$$

augmenting the local association of other small high-valence cations (*e.g.*, Al, Fe^{3+}, Cr^{3+}) at *M*(2) and *M*(3) with Al at *T*(1) and *T*(2) in accord with the valence-sum rule (Brown 1981, 2002; Hawthorne 1997; Hawthorne et al. 1998). Della Ventura et al. (1996) showed that in substitution (4), there is no short-range order involving $^{[4]}Ti$ and Si.

Therefore, the incorporation and site ordering of Ti in amphiboles is a function of both amphibole composition and conditions of crystallization. Understanding the crystal-chemical constraints on ^{C}Ti partitioning in amphiboles is of great interest as the common occurrence of the oxo component in amphiboles is becoming more apparent due to advances in the structural and analytical techniques and advancing crystal-chemical knowledge. The present work was designed to examine rigorously the ordering of Ti in a calcium amphibole for which comparative crystal-chemistry, based on X-ray diffraction data, indicates that ^{C}Ti is distributed over all the octahedrally coordinated sites.

Sample provenance

One sample was selected from the crystal-chemical database of the Pavia unit of the CNR-IGG institution, which contains the results of complete (EMP+SIMS) chemical analysis, X-ray crystal-structure refinement and in some cases Mössbauer spectroscopy. This sample was chosen because of its composition (*i.e.*, high Ti content) and the availability of large (centimetric) crystals suitable for neutron diffraction. The sample comes from a gabbro at Kaersut (Greenland), the type locality of kaersutite. The sample code at the Muséum National d'Histoire Naturelle in Paris is MHN109.991, and the crystal code in the CNR-IGG database is 632. Previous work based on comparison with X-ray refinement of synthetic high-Ti Fe-free kaersutite (Tiepolo et al. 1999) had suggested that also this sample had a significant amount of Ti at the *M*(3) site, and that it cannot be considered as an oxo-amphibole (namely, kaersutite) because its (OH+F) content, as measured by SIMS, is higher than 1.0 atoms per formula unit (*apfu*).

Experimental

- **X-ray diffraction**

Some fragments of a centimetric crystal (~ 0.8 cm^3) of the amphibole sample from Kaersut, here labelled as "K(1)", were used for this multi-methodological study.

Unit-cell dimensions of crystal K(1) were calculated from least-squares refinement of the *d* values obtained from 50 rows of the reciprocal lattice by measuring the centroid of gravity of each reflection in the range $-30 < \theta < +30°$. Intensity data were collected for the monoclinic equivalent pairs (*hkl* and *h-kl*) in the range $2 < \theta < 65°$. Intensities were then corrected for absorption, Lorentz and polarization effects, averaged and reduced to structure factors. Unit-cell dimensions and miscellaneous information pertaining to intensity-data collection and refinement are given in Table 1. Only reflections with $I_o > 3\sigma_I$ in the range $2 < \theta < 30°$ were considered as "observed" during unweighted full-matrix least-squares refinement on *F*, done with an extensively modified version of the program ORFLS (Busing and Levy 1962) which is able to deal with complex solid-solutions (Cannillo et al. 1983). Fully-ionized scattering factors of the appropriate chemical species were used for non-tetrahedrally coordinated cation sites, whereas appropriate combinations of neutral *vs.* ionized scattering-factors were used for the *T* sites and the O atoms (see Oberti et al. 1992). The electron density in the *A* cavity was modelled using three different subsites, of which only *A*(*m*) and *A*(2) are likely to be occupied by A-group cations. Site populations were derived and optimized by

combining refined site-scattering values with refined mean bond lengths, and using all the information derived from statistical treatment of the amphibole data base. More details on the procedure are given in the following sections. Refined atom coordinates and displacement parameters are given in Table 2; selected interatomic distances and angles are given in Table 3, and refined site-scattering values (Hawthorne et al. 1995) are listed in Table 4.

- **Neutron diffraction**

A crystal of K(1) (1.5 x 1.2 x 0.75 mm^3), optically free of defects and twinning, was selected under a transmitted-light polarizing microscope for the neutron-diffraction experiment. Neutron Laue data were collected at room temperature on the Laue diffractometer KOALA on the OPAL reactor at the Australian Nuclear Science and Technology Organisation. KOALA, which is essentially a clone of the Laue diffractometer VIVALDI at the Institut Laue-Langevin, Grenoble (McIntyre et al. 2006; Edwards 2011; Gatta et al. 2012), uses the Laue diffraction technique on an unmonochromated thermal-neutron beam with a large solid-angle (8 sterad) cylindrical image-plate detector to increase the detected diffracted intensity by one to two orders of magnitude compared to a conventional monochromatic experiment. The crystal was mounted with the high-symmetry axis well away from the single instrument-rotation axis, in order to avoid bias in the final refined anisotropic-displacement parameters due to the blind region in reciprocal space around the rotation axis. Twenty-nine Laue diffraction patterns, each accumulated over 60 min on average and with two different crystal orientations to ensure the best coverage of reciprocal space, were collected at 15° intervals of rotation of the K(1) crystal. Two crystal orientations were used to ensure the best coverage of reciprocal space and avoid bias in the final refined anisotropic-displacement parameters due to the blind region in reciprocal space around the single rotation axis in one orientation. Data extends to a minimum *d* spacing of ~ 0.5 Å (with λ_{min} = 0.8 Å and λ_{max} = 5.2 Å).

The Laue patterns were indexed on the basis of the unit-cell parameters previously measured by single-crystal X-ray diffraction (Table 1) and compatible with the reflection conditions of the space group *C*2/*m*, using the program LAUEGEN of the Daresbury Laboratory Laue Suite (Campbell 1995; Campbell et al. 1998), and the reflections were corrected for background and integrated using the program INTEGRATE+, which uses a two-dimensional version of the minimum $\sigma(I)/I$ algorithm (Wilkinson et al. 1988). Corrections for absorption were deemed unnecessary due to the small crystal volume and low fraction of highly absorbing elements.

Reflections were normalised to the incident wavelength, using a curve derived by comparing equivalent reflections and multiple observations, and corrected for the different angles of incidence to the detector surface via the local program LAUE4 (Piltz 2012), and $|F_O| > 4\sigma(F_O)$. Diffraction peaks were indexed on the basis of the unit-cell parameters previously measured by single-crystal X-ray diffraction (Table 1) and compatible with the reflection conditions of the space group *C*2/*m*.

Anisotropic crystal-structure refinement based on the neutron intensity data was done in the space group *C*2/*m* using the SHELX-97 software (Sheldrick 2008), starting from a structure model without any H atom included. The neutron scattering lengths of Na, Ca, Fe, Ti, Al, Si, O and H were taken from Sears (1986). Secondary isotropic extinction was corrected by the formalism of Larson (1967), as implemented in the SHELXL-97 package. The structure refinement was done with the following strategy: the *A*(*m*) site was modelled with Na alone; the *M*(1), *M*(2), and *M*(3) sites were modelled as occupied by Fe and Ti (and their fractions were mutually refined) and *M*(4) by Ca and Na (fractions mutually refined); the *T*(1) and *T*(2) sites were modelled with Al and Si (and their fractions mutually refined). Convergence was reached with one intense negative residual peak (at $x \sim 0.208$, $y \sim 0$, $z \sim 0.768$) in the final difference-Fourier map of the nuclear density. Further cycles of refinement were done with H assigned to these coordinates, and its site occupancy was refined. Refinement of all variable parameters converged with all the principal mean-square atomic displacement parameters positive, including those for the H site. The variance-covariance matrix showed no significant correlation among the refined parameters. Site coordinates and displacement parameters are listed in Table 2; selected interatomic distances and angles are given in Table 3, and refined site-scattering values and aggregate neutron-scattering lengths are listed in Table 4.

- **Microprobe analysis**

Subsequent to the collection of the X-ray intensity data, the same fragment of the crystal K(1) was mounted in epoxy, polished, and analysed by electron- and ion-microprobe techniques (for H and Li; Li was found to be at the wt ppm level) following the procedures described by Oberti et al. (1992) and Ottolini et al. (1993, 2001). Chemical compositions (Table 5) are the mean of at least 10 determinations on the same crystal; because no significant compositional zoning was observed, they should be representative of the bulk composition of the sample. Formulae were calculated on the basis of 24(O,OH,F) = 24 *apfu*. The total number of cations was adjusted so as to obtain the best fit

between the refined group-site-scattering values and those calculated from EMP analysis. Given that OH and F were measured by SIMS, this procedure implies a unique solution for the calculation of Fe^{3+} within the uncertainty of the SIMS analysis. The initial cation assignment was done as discussed by Hawthorne and Oberti (2007). This showed C-group cations (*i.e.*, Mg, Fe^{2+}, Mn^{2+}, Ni, Al, Fe^{3+}, Cr^{3+}, Ti^{4+}) in excess of 5.0 *apfu*, as is commonly the case in calcium amphiboles. What specific C-group cations should be assigned to the B-group? Usually, one assigns Mn^{2+} and Fe^{2+} in that order, using the site preference $^{M(4)}Mn^{2+} > {}^{M(4)}Fe^{2+}$ observed in monoclinic Fe-Mg-Mn amphiboles as the rationalization for this procedure. In the present case, we know the total scattering from both the B-group [≡ *M*(4) site] and the C-group [≡ *M*(1), *M*(2) and *M*(3) sites] cations, and can check the assignment on this basis. In conclusion, all Mn^{2+} was assigned to *M*(4) together with 0.73 *apfu* of Fe^{2+}. The resultant unit-formula assignment is shown in Table 5.

Results: Site assignment of cations

- **T-group cations**

Initially, the Al contents at the *T*(1) and *T*(2) sites were allowed to vary during refinement of the neutron data. However, the resultant site-populations were far too Al-rich for (1) the chemical formula of the crystal; (2) the observed <*T*(1)-O> and <*T*(2)-O> distances, and (3) the grand <*T*-O> distance. We suspected that too much scattering (all the cation sites) was being varied in the neutron refinement, leading to poor scaling, and hence we refined the structure with the site populations of the *T*(1) and (2) sites fixed at their values obtained from the X-ray structure refinement. Indeed, the <*T*(1)-O> and <*T*(2)-O> distances derived from the neutron refinement are almost identical to those obtained from the X-ray refinement. According to the systematic work reported in Oberti et al. (2007), in amphiboles the majority of ^{T}Al occurs at the *T*(1) site and only minor ^{T}Al occurs at the *T*(2) site. Moreover, the $^{T(1)}Al$ content can be obtained from the regression equation of Oberti et al. (2007) [$^{T(1)}Al = (<T(1)\text{-}O> - 1.6193) \cdot 34.2199$], which gives 1.84 *apfu*. Because the size of the *T*(2) tetrahedron depends on many compositional factors (including the Fe content), the amount of $^{T(2)}Al$ cannot be estimated quantitatively by a similar equation, and should be calculated by difference from the ^{T}Al values obtained from EMP analysis: 1.97 -1.84 = 0.13 *apfu*. Thus, *T*(1) = 2.16 Si + 1.84 Al and *T*(2) = 3.87 Si + 0.13 Al *apfu*.

- **C-group cations**

The assignment of site populations to the $M(1)$, $M(2)$ and $M(3)$ sites is the major goal of this work. Inspection of Table 5 shows that there are five cations to be assigned to these sites: Mg^{2+}, Fe^{2+}, Fe^{3+}, Al^{3+} and Ti^{4+}. We have assigned all Mn^{2+} and some Fe^{2+} to $M(4)$, as indicated by the chemical formula and the refined site-scattering values at $M(4)$. With a combination of just two different sets of diffraction data, we cannot uniquely determine site populations for five scattering species over three sites (Hawthorne 1983), and hence we must reduce this number. In terms of scattering, we may treat Fe^{2+} and Fe^{3+} as Fe, and assign ${}^{C}Al$ to $M(2)$ in accord with the known site-preference for this species in amphiboles containing significant Fe (Hawthorne and Oberti 2007; Oberti et al. 2007). This leaves three scattering species to be refined over three sites, $M(1,2,3)$.

We may write the refined site-scattering values from the X-ray and neutron-scattering experiments as follows:

$$12 \cdot {}^{Mg}a^{M(1)} + 26 \cdot {}^{Fe}a^{M(1)} + 22 \cdot {}^{Ti}a^{M(1)} = {}^{XRAY}S^{M(1)}$$
$$12 \cdot {}^{Mg}a^{M(2)} + 26 \cdot {}^{Fe}a^{M(2)} + 22 \cdot {}^{Ti}a^{M(2)} = {}^{XRAY}S^{M(2)} - 13 \cdot {}^{Al}a^{M(2)}$$
$$12 \cdot {}^{Mg}a^{M(3)} + 26 \cdot {}^{Fe}a^{M(3)} + 22 \cdot {}^{Ti}a^{M(3)} = {}^{XRAY}S^{M(3)}$$

$${}^{Mg}B \cdot {}^{Mg}a^{M(1)} + {}^{Fe}B \cdot {}^{Fe}a^{M(1)} + {}^{Ti}B \cdot {}^{Ti}a^{M(1)} = {}^{NEUTRON}S^{M(1)}$$
$${}^{Mg}B \cdot {}^{Mg}a^{M(2)} + {}^{Fe}B \cdot {}^{Fe}a^{M(2)} + {}^{Ti}B \cdot {}^{Ti}a^{M(2)} = {}^{NEUTRON}S^{M(2)} - {}^{Al}B \cdot {}^{Al}a^{M(2)}$$
$${}^{Mg}B \cdot {}^{Mg}a^{M(3)} + {}^{Fe}B \cdot {}^{Fe}a^{M(3)} + {}^{Ti}B \cdot {}^{Ti}a^{M(3)} = {}^{NEUTRON}S^{M(3)}$$

where ${}^{XRAY}S^{M(1)}$ is the refined site-scattering value for the $M(1)$ site from the refinement of the X-ray data, ${}^{NEUTRON}S^{M(1)}$ is the refined site-scattering value for the $M(1)$ site from the refinement of the neutron data, ${}^{Mg}B$ is the neutron scattering length for Mg, ${}^{Mg}a^{M(1)}$ is the amount (site population) of Mg assigned to the $M(1)$ site (etc. for the other sites and the other scattering species). Stoichiometry requires the following equations (*i.e.*, there are no vacancies at the $M(1,2,3)$ sites):

$${}^{Mg}a^{M(1)} + {}^{Fe}a^{M(1)} + {}^{Ti}a^{M(1)} = 2$$
$${}^{Mg}a^{M(2)} + {}^{Fe}a^{M(2)} + {}^{Ti}a^{M(2)} = 2 - {}^{Al}a^{M(2)}$$
$${}^{Mg}a^{M(3)} + {}^{Fe}a^{M(3)} + {}^{Ti}a^{M(3)} = 1$$

There are nine site-population variables $^{Mg}a^{M(1)}$ etc. and nine equations, and we may solve for the site populations $^{X}a^{M(n)}$ where X = Mg, Fe and Ti, and n = 1-3. The resultant values are given in Table 6. They confirm that Ti^{4+} occurs in all the three octahedrally coordinated sites in this sample (as suggested by Tiepolo et al. 1999). The unit-cell contents derived from the chemical analysis (Table 5) provide a check on the accuracy of these site populations by comparing the sums of the different scattering species assigned from the diffraction experiments with the same scattering species determined by electron-microprobe analysis, as is done in the two columns to the right in Table 6. The closeness of the two sets of compositions strongly suggests that the derived site populations are correct.

The values given in Table 6 are derived solely from the site-scattering values and do not take into account the presence of both Fe^{2+} and Fe^{3+}. We may examine this issue in terms of the geometrical parameters (mean bond-lengths and distortion) at the *M*(1), *M*(2) and *M*(3) sites, in two ways as we now describe:

1) Use optimised ideal mean bond-lengths for complete occupancy of the *M*(1,2,3) sites by Mg (2.078 Å), Fe^{2+} (2.125 Å), Fe^{3+} (2.025 Å), Ti^{4+} (1.960 Å) and Al (1.929 Å) for (OH, F, Cl) amphiboles based on the CNR-IGG database in Pavia (Oberti et al. 2007), adjusted for the effect of F at O(3) on the <*M*(1)-O> and <*M*(3)-O> distances (-0.13 F *apfu*), and taking into account the observation that significant Fe^{3+} content at the *M*(1) site causes a considerable increase in the *M*(1) octahedron distortion parameter Δ (Brown and Shannon 1973) from the common value of 2-3. The value of Δ for the *M*(1) octahedron in crystal K(1) is 2.49, thus excluding the presence of Fe^{3+} at *M*(1). With no Fe^{3+} at *M*(1), the calculated <*M*(1)-O> distance is 2.064 Å, already shorter than the refined value of 2.078 Å. Thus Fe^{3+} is either ordered at the *M*(2) site, which would lead to a calculated <*M*(2)-O> distance of 2.049 Å and a calculated <*M*(3)-O> distance of 2.069 Å (to be compared to the refined values of 2.074 Å and 2.070 Å, respectively), or is distributed between the *M*(2) and the *M*(3) sites. This latter hypothesis would make the overall shrinking of the strip of octahedra more homogeneous in crystal K(1), which is consistent with the presence of a significant oxo component. This issue will be explored further in the last section of this paper.

2) The regression equations of Hawthorne and Oberti (2007, Table 7) may be used to calculate the Fe^{3+} content of each *M*(1,2,3) site using the occupancies given in Table 6. The equation for the *M*(2) octahedron involves just the aggregate radius of the constituent *M*(2) cations, whereas the equations for the *M*(1) and *M*(3) octahedra take into account not only the aggregate radius of the constituent

318 *M*(1) and *M*(3) cations, but also the aggregate radius of the anion(s) at O(3) and the cations at *M*(4),
319 the amount of ^{T}Al and the aggregate net charge at the *A* site. The results are shown below:
320
321 *M*(1) Fe^{3+} = 0.00 *apfu*, $\langle M(1)\text{-O}\rangle_{obs}$ = 2.078 and $\langle M(1)\text{-O}\rangle_{calc}$ = 2.077 Å;
322 *M*(2) Fe^{3+} = 0.00 *apfu*, $\langle M(2)\text{-O}\rangle_{obs}$ = 2.073 and $\langle M(2)\text{-O}\rangle_{calc}$ = 2.073 Å;
323 *M*(3) Fe^{3+} = 0.10 *apfu*, $\langle M(3)\text{-O}\rangle_{obs}$ = 2.070 and $\langle M(3)\text{-O}\rangle_{calc}$ = 2.070 Å.
324
325 This gives a significantly lower Fe^{3+} content than that obtained by formula recalculation with the
326 constrain of H and F measured by SIMS (*i.e.*, 0.33 *apfu*). The predicted <*M*-O> values have
327 standard errors of estimate of 0.0027, 0.0053 and 0.0058 Å for *M*((1), *M*(2) and *M*(3), respectively,
328 which at their limits would predict a further Fe^{3+} content of 0.023 Fe^{3+}. Anyway, these results
329 indicate that Fe^{3+} is strongly ordered at the *M*(3) site and is in reasonable accord with
330 electroneutrality using the neutron-derived H content of 1.02(2) *apfu*.
331 The presence of a significant amount of Ti^{4+} at the *M*(1) site is usually detected by a much
332 higher value of the anisotropic displacement parameters (*adp*) refined at this site than at the *M*(2)
333 and *M*(3) sites, indicating a shift of the Ti^{4+} ions toward the edge of the octahedron connecting the
334 two O(3) sites (Tiepolo et al. 1999). In some cases, two split positions, *M*(1) and *M*(1'), can even be
335 refined (*e.g.*, Hawthorne et al. 2000). In this work, a higher value of the *adp* at *M*(1) and *M*(3) was
336 obtained from the X-ray data but not from the neutron data. The presence of Ti^{4+} at *M*(1), *M*(2) and
337 *M*(3), as well as the presence of significant F, may be the reason for the unusual distortion pattern of
338 the ribbon of octahedra observed in crystal K(1), which is generally more shrunk than expected
339 based on the ideal <cat-O> distances used in the crystal-chemical analysis of amphiboles (cf. Oberti
340 et al. 2007 and the discussion above).
341
342 - **B-group cations**
343 Although two different subsites (*i.e.*, *M*(4) and *M*(4'); Table 2) can be refined from X-ray
344 data due to the oblong shape of the electron density, their distance is close to the resolution of the
345 data. Hence, the total scattering obtained is more accurate than that based on the refinement of a
346 unique position, but its partitioning cannot be considered accurate. However, inspection of the cat-O
347 distances and comparison with the shape of the electron density found in many other amphibole
348 compositions show that smaller cations (Mg, Fe^{2+}, Mn^{2+}) order at the *M*(4') position (Oberti et al.

2007). Cations were assigned to the B-group in the usual fashion (*e.g.*, Hawthorne et al. 2012). Those C-group cations in excess of 5 *apfu* were assigned as B-group cations in the following sequence: Mn^{2+}>Fe^{2+}>Mg, and all Ca was assigned to this site until the site is completely occupied (Hawthorne et al. 2012). The resultant calculated X-ray/neutron site-scattering values (Table 4) are in close agreement with the analogous refined values for both the X-ray and neutron refinements.

- **A-group cations**

The site populations at the *A*(*m*), *A*(2) and *A* sites were refined unconstrained in both X-ray and neutron refinements. Although the model used for neutron data includes only the *A*(*m*) subsite, as the *A* and *A*(2) site populations were found not to be significant, the aggregate refined scattering/neutron-scattering value in the A cavity is close to that calculated from the A-group cations based on electron- and ion-microprobe analysis (Table 4). The higher value obtained by X-rays structure refinement may be due to the relatively high values of the atomic displacement parameters (Table 2).

- **W-group anions**

The site population of the H site was refined directly in the neutron structure refinement, with convergence to the following value: 1.02(2) H + 0.98 □ a*pfu.* This may be compared to the value derived by SIMS of 0.87 H *apfu*. Ottolini and Hawthorne (2001) give an uncertainty of 5-10% for the determination of H by SIMS for the analytical method used here, *i.e.*, 0.04-0.09 *apfu* for crystal K(1). The upper limit of the uncertainty plus the standard deviation of the H value derived by neutron scattering suggest that there is little significant difference between these two values.

Discussion and conclusions

- **Hydrogen bonding**

The neutron structure refinement provides a clear picture of the H site location, anisotropic displacement regime and potential H-bonding configuration. The coordinates of the H site obtained in this study are consistent with previous experimental findings based on single-crystal neutron structure refinement reported by Pechar et al. (1989) for a kaersutite from Bohemia. The refined O-H bond distance of this study is 0.951(2) Å (Table 3), whereas that reported by Pechar et al. (1989)

is 0.93(1) Å. A correction for the "riding motion effect" (following the protocol of Busing and Levy 1964) gives 0.982 Å (Table 3), showing that the O–H distance is significantly affected by the motion of the proton. The magnitude and orientation of the displacement ellipsoid of the H site of this study is shown in Fig. 2, along with the potential H-bonding network. The shape of the ellipsoid (root-mean-square components: *R*1:*R*2:*R*3 = 1.89:1.84:1, with *R*1 and *R*2 dispersed on (100), Fig. 2) is strongly influenced by the geometry of the weak interactions with the oxygens of the two independent tetrahedra. Inspection of the difference-Fourier map of the nuclear density does not show any evidence of splitting of the H site. Pechar et al. (1989) did not report any indication of possible hydrogen bonding. However, our data lead us to consider that at least three potential weak H-bonds may occur: with O(6) x 2 and O(7) as *acceptors* (*i.e.*, H···O(6)= 2.763(2) Å, O(3)···O(6) =3.316(1) Å and O(3)–H···O(6) =117.86(1)°; H···O(7)= 2.694(3) Å, O(3)···O(7) = 3.270(2) Å and O(3)–H···O(7) = 119.6(2)°, Table 3). A similar trifurcated configuration is observed in trioctahedral phyllosilicates, in which the *donor* is an oxygen site shared by three adjacent octahedra (belonging to the octahedral sheet) and the *acceptors* are oxygens of the superimposed 6-membered ring of tetrahedra (belonging to the tetrahedral sheet) (*e.g.*, Gatta et al. 2011, 2013, 2014). In all these cases, the O_{donor}–H···$O_{acceptor}$ angles range between 115-140°.

- **The relation between $^{[6]}Ti^{4+}$ and $^{O(3)}O^{2-}$**

The Mg-Fe-Ti site populations of the C cations calculated from the refined X-ray and neutron site-scattering values are in excellent agreement with the analysed chemical compositions (Table 6). Ti^{4+} is preferentially ordered at the *M*(1) site, in accord with the dominance of substitution (2) (see above). The refined Ti^{4+} content of *M*(1) is 0.38 *apfu* (Table 6); using the neutron site population for hydrogen at the H site, the site population of O(3) is 1.02 $(OH)^-$ + 0.20 F^- + 0.78 O^{2-}. These values, $^{M(1)}Ti^{4+}$ = 0.38 *apfu* and $^{O(3)}O^{2-}$ = 0.78 *apfu*, are in almost exact accord with substitution (2), suggesting that the incorporation of O^{2-} at O(3) is controlled by the occurrence of Ti^{4+} at *M*(1), and the bond-valence requirements of Ti^{4+} at *M*(1) are met primarily by very short bonds to O^{2-} at the O(3) site.

However, there is significant Ti^{4+} at the *M*(2) and *M*(3) sites (Table 6). Incorporation of Ti^{4+} at the *M*(2) site is a result of substitution (3) and is unrelated to dehydrogenation in amphiboles. The incorporation of Ti^{4+} at *M*(3) is more problematic. Incorporation of Ti^{4+} at *M*(3) could in principle be related to dehydrogenation as the *M*(3) site is also coordinated by two O(3) sites. However, in

amphibole K(1), all O^{2-} at O(3) is associated with Ti^{4+} at *M*(1), and Ti^{4+} at *M*(3) cannot be associated independently with O^{2-} at O(3) as all O^{2-} at O(3) is already associated with Ti^{4+} at *M*(1). This being the case, it is not clear how the bond-valence requirements of Ti^{4+} at *M*(3) can be satisfied. Possibly, $^{M(3)}Ti^{4+}$ could be incorporated into the amphibole structure by, for example, a substitution such as $^{M(3)}Ti^{4+} + 2\ ^{M(2)}Mg^{2+} \rightarrow {}^{M(3)}Mg^{2+} + 2Al^{3+}$, that is locally spatially associated with substitution (2), such that $^{M(3)}Ti^{4+}$ bonds to $^{O(3)}O^{2-}$. An analogous mechanism could also account for the occurrence of Fe^{3+} at *M*(3).

The Ti^{4+} content at the *M*(1) site compensates for 0.76 *apfu* O^{2-} at O(3). This leaves a difference of 0.02 (0.78 – 0.76 from the neutron H-site occupancy) to 0.17 *apfu* (0.93 – 0.76 from the SIMS H content) to be compensated by additional substitutions. Given the chemical formula of the sample, two possibilities remain: (1) the additional positive charge is provided by half the Ti^{4+} occurring at *M*(3), which implies substitution (6) below:

$$^{M(3)}Ti^{4+} + 2\ ^{O(3)}O^{2-} \rightarrow {}^{M(3)}Mg^{2+} + 2\ ^{O(3)}(OH)^{-} \quad (6),$$

or (2) the additional positive charge is provided by up to 0.17 Fe^{3+} *apfu* occurring at *M*(3) according to substitution (7):

$$^{M(3)}Fe^{3+} + {}^{O(3)}O^{2-} \rightarrow {}^{M(3)}Fe^{2+} + {}^{O(3)}(OH)^{-} \quad (7).$$

Note that substitution (7) is common in oxo-amphiboles where the Ti content is low or dehydrogenation has occurred after crystallization (*e.g.*, Oberti et al. 2016).

Above, we considered two approaches concerning the amount and distribution of Fe^{3+} at the *M*(1), *M*(2) and *M*(3) sites. Both exclude the presence of Fe^{3+} at the *M*(1) site and are compatible with the occurrence of Fe^{3+} at the *M*(3) site. In this regard, crystal K(1) is unusual as dehydrogenation of Fe-rich amphiboles generally proceeds according to substitution (8) below:

$$^{M(1)}Fe^{3+} + {}^{O(3)}O^{2-} \rightarrow {}^{M(1)}Fe^{2+} + {}^{O(3)}(OH)^{-} \quad (8)$$

The second approach predicts 0.13 *apfu* Fe^{3+} at *M*(3), within the range 0.02-0.17 *apfu* required by electroneutrality, highlighting the unusual nature of this amphibole.

Acknowledgements

The authors thank the Bragg Institute, Australian Nuclear Science and Technology Organization, for the allocation of neutron beam time. Financial support for FCH was provided by a Canada Research Chair in Crystallography and Mineralogy, Discovery Grants from the Natural Sciences

and Engineering Research Council of Canada, and by Canada Foundation for Innovation Grants. Two anonymous reviewers are thanked for the constructive suggestions.

References

Brown ID (1981) The bond-valence method: an empirical approach to chemical structure and bonding. In M. O'Keeffe and A. Navrotsky, Eds., Structure and Bonding in Crystals, Vol. 2, 1–30. Academic Press, New York.

Brown ID (2002) The chemical bond in inorganic chemistry. The Bond Valence Model. Oxford University Press, U.K.

Brown ID, Shannon RD (1973) Empirical bond strength–bond lengths curves for oxides. Acta Crystallogr A29:266-282.

Busing WR, Martin KO, Levy HA (1962) ORFLS. Report ORNL-Tm-305.- Oak Ridge Natl. Lab. Oak Ridge, Tn.

Busing WR, Levy HA (1964) The effect of thermal motion on the estimation of bond lengths from diffraction measurements. Acta Crystallogr 17:142-146.

Campbell JW (1995) LAUEGEN, an X-windows-based program for the processing of Laue diffraction data. J Appl Crystallogr 28:228-236.

Campbell JW, Hao Q, Harding MM, Nguti ND, Wilkinson C (1998) LAUEGEN version 6.0 and INTLDM. J Appl Crystallogr 31:496-502.

Cannillo E, Germani G, Mazzi F (1983) New crystallographic software for Philips PW11000 single crystal diffractometer. CNR Centro di Studio per la Cristallografia, Internal Report 2.

Della Ventura G, Robert JL, Bény JM (1991) Tetrahedrally coordinated Ti^{4+} in synthetic Ti-rich potassic richterites: evidence from XRD, FTIR and Raman study. Am Mineral 76:1134-1140.

Della Ventura G, Robert JL, Bény JM, Raudsepp M, Hawthorne FC (1993) The OH-F substitution in Ti-rich potassium-richterites: Rietveld structure refinement and FTIR and micro-Raman spectroscopic studies of synthetic amphiboles in the system K_2O-Na_2O-CaO-MgO-SiO_2-TiO_2-H_2O-HF. Am Mineral 78:980-987.

Della Ventura G, Robert JL, Hawthorne FC, Prost R (1996) Short-range disorder of Si and Ti in the tetrahedral double-chain unit of synthetic Ti-bearing potassium-richterite. Am Mineral 81: 56-60.

Della Ventura G, Oberti R., Hawthorne FC, Bellatreccia F (2007) FTIR spectroscopy of Ti-rich pargasites from Lherz and the detection of O^{2B} at the anionic O3 site in amphiboles. Am Mineral 92, 1645-1651.

Edwards AJ (2011) Neutron Diffraction: Recent Applications to Chemical Structure Determination. Austral J Chem 64:869–872.

Gatta GD, McIntyre GJ, Sassi R, Rotiroti N, Pavese A (2011) Hydrogen-bond and cation partitioning in 2M_1-muscovite: A single-crystal neutron-diffraction study at 295 and 20 K. Am Mineral 96:34–41.

Gatta GD, McIntyre GJ, Bromiley G, Guastoni A, Nestola F (2012) A single-crystal neutron diffraction study of hambergite, $Be_2BO_3(OH,F)$. Am Mineral 97:1891–1897.

Gatta GD, Merlini M, Valdrè G, Liermann H-P, Nénert G, Rothkirch A, Kahlenberg V, Pavese A (2013) On the crystal structure and compressional behaviour of talc: a mineral of interest in petrology and material science. Phys Chem Minerals 40:145-156.

Gatta GD, Nénert G, Guastella G, Lotti P, Guastoni A, Rizzato S (2014) A single-crystal neutron and X-ray diffraction study of a Li,Be-bearing brittle mica. Min Mag 78:55–72.

Hawthorne FC (1983) Quantitative characterization of site occupancies in minerals. Am Mineral 68:287-306.

Hawthorne FC (1997) Short-range order in amphiboles: A bond-valence approach. Can Mineral 35:201–216.

Hawthorne FC, Ungaretti L, Oberti R (1995) Site populations in minerals: terminology and presentation of results of crystal-structure refinement. Can Mineral 33:907-911.

Hawthorne FC, Oberti R, Zanetti A, Czamanske GK (1998) The role of Ti in hydrogen-deficient amphiboles: Sodic-calcic and sodic amphiboles from Coyote Peak, California. Can Mineral 36:1253-1265.

Hawthorne FC, Cooper MA, Grice JD, Ottolini L (2000) A new anhydrous amphibole from the Eifel region, Germany: Description and crystal structure of obertiite, $NaNa_2(Mg_3Fe^{3+}Ti^{4+})Si_8O_{22}O_2$. Am Mineral 85: 236–241.

Hawthorne FC, Oberti R (2007) Amphiboles: Crystal chemistry. Rev Mineral Geochem 67:1-54.

Hawthorne FC, Oberti R, Harlow GE, Maresch W, Martin RF, Schumacher JC, Welch MD (2012) Nomenclature of the amphibole super-group. Am Mineral 97:2031-2048.

503 Kitamura M, Tokonami M, Morimoto N (1975) Distribution of Ti in oxy-kaersutite. Contr
504 Mineral Petrol 51:167-172.
505 Konzett J (1997) Phase relations and chemistry of Ti-rich K-richterite-bearing mantle
506 assemblages: an experimental study to 8 GPa in a Ti-KNCMASH system. Contrib Mineral Petrol
507 128:385-404.
508 Konzett J, Sweeney RJ, Thompson AB, Ulmer P (1997) Potassium amphibole stability in
509 the upper mantle: an experimental study in a peralkaline KNCMASH system to 8.5 GPa. J Petrol
510 38: 537-568.
511 Larson AC (1967) Inclusion of secondary extinction in least-squares calculations. Acta
512 Crystallogr 23:664 – 665.
513 Leake BE (1968) A catalog of analysed calciferous and subcalciferous amphiboles together
514 with their nomenclature and associated minerals. Geol Soc Am Spec Paper 98, 210p.
515 McIntyre GJ, Lemée-Cailleau MH, Wilkinson C (2006) High-Speed Neutron Laue Diffraction
516 Comes of Age. Physica B 385-386:1055-1058.
517 Oberti R, Ungaretti L, Cannillo E, Hawthorne FC (1992) The behaviour of Ti in amphiboles: I.
518 Four- and six-coordinated Ti in richterite. Eur J Mineral 4:425-439.
519 Oberti R, Hawthorne FC, Cannillo E, Cámara F (2007) Long-range order in amphiboles.
520 Rev Mineral Geochem 67:125-171.
521 Oberti R, Boiocchi M, Zema M, Della Ventura G (2016) Synthetic potassic-ferro-richterite:
522 1. Composition, crystal structure refinement and H*T* behavior by *in operando* single-crystal X-ray
523 diffraction. Can Mineral (*in press*).
524 Ottolini L, Hawthorne FC (2001) SIMS ionization of hydrogen in silicates: A case study of
525 kornerupine. J Anal At Spectrom 16:1266–1270.
526 Ottolini L, Bottazzi P, Vannucci R (1993) Quantification of Li, Be and B in silicates by
527 secondary ion mass spectrometry using conventional energy filtering. Anal Chem 65:1960–1968.
528 Pechar F, Fuess H, Joswig W (1989) Refinement of the crystal structure of kaersutite
529 (Vlcíhora, Bohemia) from neutron diffraction. Neues Jahrb Mineral Monat 89:137-143.
530 Piltz RO (2011) Accurate data analysis for the Koala and VIVALDI neutron Laue
531 diffractometers. Abstracts of the XXII IUCr Congress, Madrid (Spain) 22-30 August 2011. Acta
532 Crystallogr A67:C155.

Saxena SK, Ekström TK (1970) Statistical chemistry of calcic amphibole. Contrib Mineral Petrol 26:276-284.

Sears, V.F. (1986) Neutron Scattering Lengths and Cross-Sections. In K. Sköld and D.L. Price, Eds., Neutron Scattering, Methods of Experimental Physics, Vol. 23A, 521-550. Academic Press, New York.

Sheldrick, G.M. (2008) A short history of SHELX. Acta Crystallogr A64:112-122.

Tiepolo M, Zanetti A, Oberti R (1999) Detection, crystal-chemical mechanisms and petrological implications of $^{[6]}Ti^{4+}$ partitioning in pargasite and kaersutite. Eur J Mineral 11:345-354.

Wilkinson C, Khamis HW, Stansfield RFD, McIntyre GJ (1988) Integration of single-crystal reflections using area multidetectors. J Appl Crystallogr 21:471-478.

Wilshire HG, Meyer CE, Nakata JK, Calk LC, Shervais JW, Nielson JE, Schwarzman EC (1988) Mafic and ultramafic xenoliths from volcanic rocks of the Western United States. U.S. Geological Survey Professional Paper, 1443, 179 pp.

549 Table 1. Summary of crystallographic, data collection and structure
550 refinement information.
551

	K(1) X-ray	K(1) neutron*
a (Å)	9.882(4)	9.882(4)
b (Å)	18.084(7)	18.084(7)
c (Å)	5.312(1)	5.312(1)
β (°)	105.26(6)	105.26(6)
V (Å^3)	915.84	915.84
Space group	*C*2/*m*	*C*2/*m*
Z	2	2
Crystal size (mm)	0.75 x 0.43 x 0.22	2.0 x 1.5 x 0.9
Rad./mono.	Mo*K*α	Thermal neutrons / Laue, (λ_{min}=0.8, λ_{max} =5.2 Å)
No. of reflections	16801	31909
Unique reflections	1254	3099
Unique observed reflections	1210	2261
d_{min} (Å)	0.7	0.5
R_{sym}%	3.70	6.13
No. of refined parameters	129	116
**$R_1(F)$ %	1.78	5.25
R_{all} %	2.28	7.45
Maximum residual peaks	***0.47 e-/Å^3	+2.1/-2.8 fm/Å^3

*Cell dimensions taken from X-ray data; **$R_1(F)$ % calculated on the basis of $F_O > 3\sigma(F_O)$ for the X-ray data and $F_O > 4\sigma(F_O)$ for the neutron data; ***close to the *M*(1) site, can be attributed to the ordering of Ti^{4+}.

552
553
554
555
556
557
558
559
560
561
562
563
564
565

Table 2. Atom coordinates and displacement parameters (Å^2) for the amphibole of this work.

Site	*x*	*y*	*z*	U^{11*}	U^{22*}	U^{33*}	U^{12*}	U^{13*}	U^{23*}	U^{eq*}
K(1) – X–ray										
T(1)	0.28234(5)	0.08503(3)	0.30227(10)	0.0058(2)	0.0066(2)	0.0066(2)	–0.0009(2)	0.0007(2)	–0.0003(2)	0.0065(2)
T(2)	0.29067(5)	0.17235(3)	0.81009(9)	0.0056(2)	0.0075(2)	0.0060(2)	–0.0009(2)	0.0011(2)	0.0001(2)	0.0064(2)
M(1)	0	0.08646(4)	½	0.0098(3)	0.0176(3)	0.0081(3)	0	0.0040(2)	0	0.0115(2)
M(2)	0	0.17730(4)	0	0.0065(4)	0.0073(3)	0.0067(4)	0	0.0018(2)	0	0.0068(2)
M(3)	0	0	0	0.0102(5)	0.0073(5)	0.0086(5)	0	–0.0009(3)	0	0.0093(3)
M(4)	0	0.27936(3)	½	0.0115(3)	0.0078(3)	0.0113(3)	0	0.0068(2)	0	0.0095(2)
M(4')	0	0.2621(3)	½	0	0	0	0	0	0	0.0171(10)
A	0	½	0	0.076(7)	0.021(4)	0.076(7)	0	0.074(7)	0	0.048(4)
A(*m*)	0.0537(7)	½	0.1067(12)	0.053(3)	0.025(2)	0.047(3)	0	0.036(3)	0	0.037(2)
A(2)	0	0.4737(5)	0	0.051(5)	0.037(4)	0.079(7)	0	0.055(5)	0	0.049(4)
O(1)	0.10776(13)	0.08645(7)	0.2191(3)	0.0078(6)	0.0128(7)	0.0093(6)	–0.0012(4)	0.0017(5)	–0.0001(5)	0.0101(4)
O(2)	0.11914(13)	0.17219(7)	0.7283(3)	0.0073(6)	0.0114(5)	0.0098(6)	–0.0004(4)	0.0014(4)	0.0009(5)	0.0097(3)
O(3)	0.1082(2)	0	0.7150(4)	0.0092(8)	0.0156(8)	0.0136(9)	0	0.0021(7)	0	0.0130(5)
O(4)	0.3656(2)	0.24973(8)	0.7864(3)	0.0140(6)	0.0109(7)	0.0120(6)	–0.0027(5)	0.0037(5)	0.0008(5)	0.0123(4)
O(5)	0.34973(14)	0.13938(8)	0.1091(3)	0.0094(6)	0.0167(7)	0.0130(6)	–0.0005(5)	0.0012(5)	0.0051(5)	0.0134(4)
O(6)	0.34609(14)	0.11660(8)	0.6080(3)	0.0094(6)	0.0167(7)	0.0150(6)	0.0009(5)	0.0027(5)	–0.0051(5)	0.0138(4)
O(7)	0.3428(2)	0	0.2782(4)	0.0119(9)	0.0157(10)	0.0206(11)	0	0.0015(8)	0	0.0166(6)
K(1)–Neutron										
T(1)	0.28216(6)	0.08500(3)	0.30226(12)	0.0052(2)	0.0060(2)	0.0060(2)	–0.0006(1)	0.0006(2)	–0.0006(1)	0.0059(2)
T(2)	0.29056(5)	0.17238(3)	0.81021(11)	0.0059(2)	0.0065(2)	0.0060(2)	–0.0009(1)	0.0012(2)	0.0003(1)	0.0062(1)
M(1)	0	0.09012(3)	½	0.0074(3)	0.0023(2)	0.0059(3)	0	0.0016(2)	0	0.0052(2)
M(2)	0	0.17697(3)	0	0.0071(3)	0.0069(2)	0.0068(3)	0	0.0018(2)	0	0.0069(2)

M(3)	0	0	0	0.0070(3)	0.0062(3)	0.0056(4)	0	0.0016(3)	0	0.0063(2)
M(4)	0	0.27828(4)	½	0.0119(3)	0.0145(3)	0.0112(3)	0	0.0065(3)	0	0.0119(2)
A(*m*)	0.0369(7)	½	0.0762(13)	0.089(7)	0.118(5)	0.093(6)	0	0.077(5)	0	0.090(3)
O(1)	0.10791(4)	0.08643(2)	0.21876(9)	0.0074(2)	0.0119(2)	0.0095(2)	–0.0012(1)	0.0012(1)	–0.0001(1)	0.0098(1)
O(2)	0.11925(4)	0.17211(2)	0.72815(8)	0.0066(2)	0.0104(1)	0.0095(2)	–0.0002(1)	0.0008(1)	0.0012(1)	0.0091(1)
O(3)	0.10828(6)	0	0.71491(13)	0.0095(2)	0.0142(2)	0.0148(3)	0	0.0013(2)	0	0.0132(1)
O(4)	0.36545(5)	0.24984(2)	0.78717(9)	0.0136(2)	0.0093(2)	0.0121(2)	–0.0029(1)	0.0035(2)	0.0001(1)	0.0116(1)
O(5)	0.34970(4)	0.13944(2)	0.10881(9)	0.0099(2)	0.0157(2)	0.0118(2)	–0.0009(1)	0.0010(2)	0.0050(1)	0.0128(1)
O(6)	0.34592(4)	0.11669(2)	0.60790(9)	0.0106(2)	0.0151(2)	0.0140(2)	0.0005(1)	0.0027(2)	–0.0057(1)	0.0134(1)
O(7)	0.34272(7)	0	0.27894(14)	0.0126(3)	0.0139(2)	0.0210(3)	0	0.0020(2)	0	0.0163(1)
H	0.2080(3)	0	0.7672(7)	0.013(1)	0.044(2)	0.045(2)	0	0.004(1)	0	0.034(1)

* for *K(1) – X–ray*, the U^{ij} values are calculated from the refined β^{ij} values. The atom- displacement parameter takes the form: exp [$-2\pi^2$ ($h^2a^{*2}U^{11} + k^2b^{*2}U^{22} + l^2c^{*2}U^{33} + 2\ hka^*b^*U^{12} + 2\ hla^*c^*U^{13} + 2\ klb^*c^*U^{23}$)].

Table 3. Selected interatomic distances (Å) and angles (°) for the amphibole of this work.

	X-ray	Neutron		X-ray	Neutron
T(1)–O(1)	1.665(2)	1.661(1)	*T*(2)–O(2)	1.635(2)	1.633(1)
T(1)–O(5)	1.680(2)	1.683(1)	*T*(2)–O(4)	1.604(2)	1.604(1)
T(1)–O(6)	1.680(2)	1.680(1)	*T*(2)–O(5)	1.653(2)	1.651(1)
T(1)–O(7)	1.667(1)	1.666(1)	*T*(2)–O(6)	1.667(2)	1.667(1)
<*T*(1)–O>	1.673	1.673	<*T*(2)–O>	1.640	1.639
M(1)–O(1) x2	2.049(1)	2.052(1)	*M*(2)–O(1) x2	2.130(2)	2.125(1)
M(1)–O(2) x2	2.123(2)	2.075(1)	*M*(2)–O(2) x2	2.091(1)	2.092(1)
M(1)–O(3)	2.062(1)	2.112(1)	*M*(2)–O(4) x2	2.000(2)	2.002(1)
<*M*(1)–O>	2.078	2.080	<*M*(2)–O>	2.073	2.073
M(3)–O(1) x4	2.069(1)	2.068(1)	*A*-O(5) x4	3.058(2)	
M(3)–O(3) x2	2.071(2)	2.072(1)	*A*-O(6) x4	3.071(2)	
<*M*(3)–O>	2.070	2.070	*A*-O(7) x2	2.410(2)	
			<*A*-O>	2.846	
A(*m*)–O(5) x2	3.026(2)	3.027(4)			
A(*m*)–O(6) x2	2.633(2)	2.754(5)	*M*(4)–O(2) x2	2.421(2)	2.407(1)
A(*m*)–O(7)	2.485(2)	2.435(7)	*M*(4)–O(4) x2	2.328(2)	2.328(1)
A(*m*)–O(7)	2.516(2)	2.481(6)	*M*(4)–O(5) x2	2.656(2)	2.667(1)
<*A*(*m*)–O>	2.720	2.746	*M*(4)–O(6) x2	2.577(2)	2.591(1)
			<*M*(4)–O>	2.495	2.523
A(2)–O(5) x2	2.679(2)				
A(2)–O(6) x2	2.766(2)		*M*(4')–O(2) x2	2.180(1)	
A(2)–O(7) x2	2.456(2)		*M*(4')–O(4) x2	2.278(2)	
<*A*(2)–O>	2.634		*M*(4')–O(5) x2	2.840(2)	
			M(4')–O(6) x2	2.811(2)	
			<*M*(4')–O>	2.527	
O(3)–H		0.951(2)	O(3)–H···O(6) x2		117.86(1)
O(3)–H*		0.982	H···O(7)		2.694(3)
H···O(6)		2.763(2)	O(3)···O(7)		3.270(2)
O(3)···O(6)		3.316(1)	O(3)–H···O(7)		119.6(2)

*Bond distances corrected for riding motion effect following Busing and Levy (1964).

Table 4. Site-scattering values refined for the amphibole of this work.

	X-ray (*epfu*)		Neutron (barns *pfu*)
Site	Refined	EMPA	Refined
M(1)	34.08		9.144
M(2)	30.83		10.487
M(3)	17.62		5.120
Sum C	82.53	82.62	24.75
M(4)	36.45		
M(4')	4.14		
Sum B	40.59	40.52	9.53
A(*m*)	6.14		
A(2)	4.26		
A	2.55		
Sum A	12.96	12.64	3.69

Table 5. Chemical composition (wt.%) and unit formula (*apfu*) derived from EMP and SIMS analysis (H, F) of crystal K(1). *bdl* = below detection limit.

SiO_2	39.99(47)
TiO_2	6.07(11)
Al_2O_3	12.02(24)
Cr_2O_3	0.02(2)
*Fe_2O_3	2.88
*FeO	6.77
MnO	0.13(2)
NiO	0.02(2)
MgO	13.50(22)
CaO	12.19(23)
Na_2O	2.50(15)
K_2O	0.93(4)
H_2O	0.86
F	0.42(5)
Cl	*bdl*
-O=F	0.18
Total	98.13
Si	6.031
Al	1.969
sum T	8.000
Al	0.168
Fe^{3+}	0.327
Ti	0.688
Cr	0.002
Ni	0.002
Mg	3.032
Fe^{2+}	0.781
sum C	5.000
Fe^{2+}	0.073
Mn^{2+}	0.017
Ca	1.910
sum B	2.000
Ca	0.060
Na	0.731
K	0.179
sum A	0.970
OH	0.865
F	0.200
O	0.935
sum W	2.000
Note: *FeO_{tot} = 9.36(31) wt%; OH and F were measured by SIMS, this procedure implies a unique solution for the calculation of Fe^{2+}/Fe^{3+}. Li was found to be at the wt ppm level.	

Table 6. Site populations (*apfu*) derived from X-ray and neutron site-scattering refinements for the amphibole of this work

	M(1)	*M*(2)	*M*(3)	Σ	EMPA
Mg	1.17	1.28	0.55	3.00	3.03
Fe	0.45	0.39	0.29	1.13	1.11
Ti	0.38	0.16	0.16	0.70	0.69
Al	-----	0.17	-----	0.17	0.17
Σ	2.00	2.00	1.00	5.00	5.00

Figure 1. Projection onto (100) of the structure of amphibole K(1). The site nomenclature is also shown. Structure model based on the neutron refinement of this study; displacement probability factor: 50%.

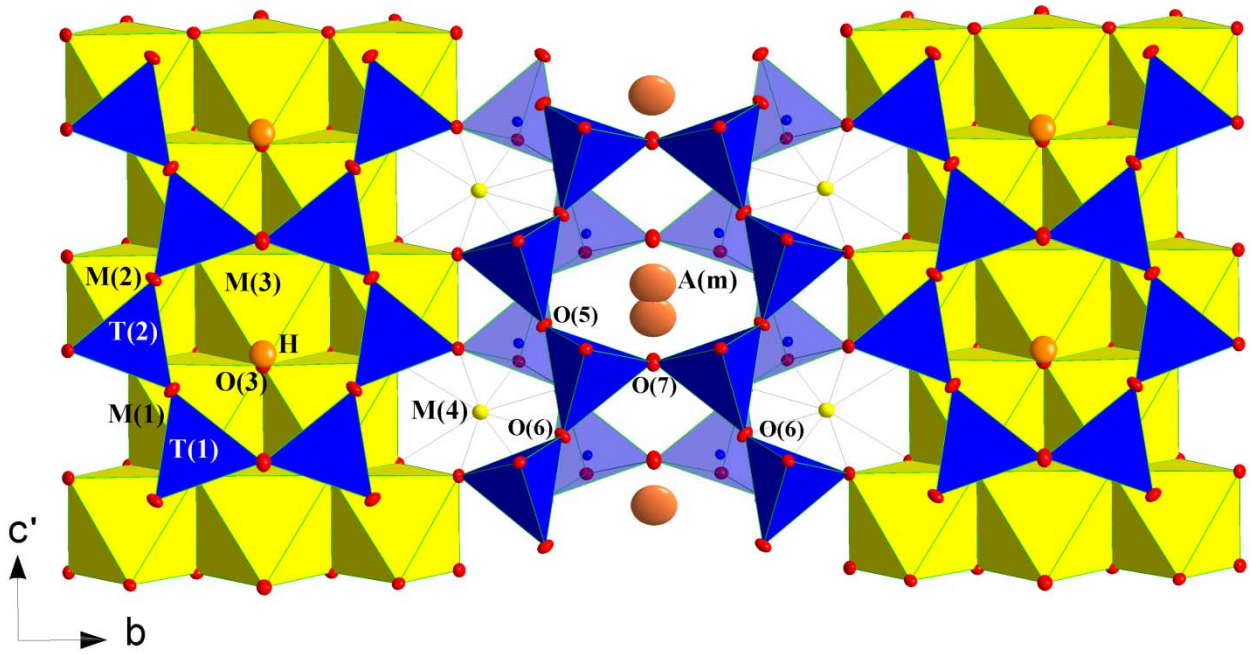

Figure 2. H-bonding configuration in the structure of K(1) amphibole deduced on the basis of the neutron structure refinement of this study. Displacement probability factor: 50%.